

Trapping mechanism and sites of H and D atoms in solid Ne

Yu.A. Dmitriev

Ioffe Institute, 26 Politekhnicheskaya Str., St. Petersburg 194021, Russia
E-mail: dmitrievyurij@gmail.com

N.P. Benetis

*Department of Environmental Engineering and Antipollution Control, Technological Educational Institute
of Western Macedonia (TEI), Kila 50 100 Kozani, Greece*

Received January 17, 2019, published online April 26, 2019

The shifts of the isotropic Fermi contact hyperfine interactions (FCHFI) of hydrogen or deuterium atoms isolated in crystalline noble gases at cryogenic temperatures are compared to the values of the same quantities of the hydrogen atom in the gas phase. New experimental FCHFI values of H/D trapped in crystalline Ne are compared with experimentally obtained and theoretically computed values. The possible trapping sites in the distorted solid Ne gas crystalline structure occupied by the hydrogen atomic impurities are identified by the variation of the FCHFI shifts in the EPR spectra and discussed after their dependence to the deposition method. The present EPR investigation revealed formation of H₂ microcrystals in solid Ne even at a very low H₂ impurity content of 0.01% in the deposited H₂:Ne gaseous mixture.

Keywords: EPR spectra, hydrogen, deuterium, solid Ne.

Introduction

Attempts of various research groups in the past to obtain H and D atoms matrix-isolated in solid Ne using gas phase condensation proved to be unsuccessful. In a classical EPR study by Foner *et al.* [1], Ne was the only matrix of inert gas which could not be doped with hydrogen atoms utilizing deposition on a cryogenic substrate at 4.2 K. Lowering temperature to 2 K as well as substitution of the light H for the heavier D did not help. Eventually, trapped H atoms were obtained by photolysis of 1% HI precursor dissolved in solid Ne. Only one trapping site was observed in that case, which yielded the following relative matrix shift of the H-atom hyperfine constant (HFC).

$$\frac{\Delta A_H}{A_H^{\text{free}}} \equiv \frac{A_H - A_H^{\text{free}}}{A_H^{\text{free}}} = +0.0043 \text{ (or 0.43\%)} \quad (1)$$

Here, $A_H^{\text{free}} = 1420.40573(5)$ MHz, is the HFC of the free (gaseous phase) hydrogen atom.

VUV optical absorption of H and D impurities in Ar and Ne films was reported by Baldini [2]. Hydrogen and deuterium atoms were produced by applying gas discharge either to the H₂ (D₂) gas alone or to Ar (or Ne) containing a small fraction of H₂ (or D₂). The gaseous flows were

deposited on a LiF substrate at 5 K. The author failed to observe H atom spectra in Ne film. Very broad and weak absorption between 10 and 11 eV in Ne films doped with D did not allow attributing this feature to atomic deuterium with certainty, neither make any reliable measurement of the spectrum.

Bondybey and Pimentel [3] studied the infrared absorption spectra of inert gas–hydrogen matrix samples which were deposited after the gas mixture passed through a glow discharge. They reported spectrum parameters for H and D in Ar and Kr and failure to observe absorption in the neon matrix experiments.

Böhmer and co-authors showed [4] that hydrogen atoms in neon as well as in other matrices may be obtained by direct photolysis of H₂ trapped in a matrix. They employed white light source with wavelengths from 400 Å to 1000 Å. The authors recorded the Lyman series of atomic hydrogen. Discussing possible trapping sites they did not come to any certain conclusion.

EPR spectra of H and D in Ne were recorded by Knight and colleagues [5]. The spin-pair interaction between H (D) atoms forming higher spin multiplets were studied theoretically and experimentally in that work as well. One trapping site was observed for each isotope with EPR parameters as fol-

lows: $A_H = 1426,0(2)$ MHz, $(\Delta A_H)/A_H^{\text{free}} = +0,394(14)\%$, $g_H = 2,0020(1)$, $A_D = 219,0(1)$ MHz, $(\Delta A_D)/A_D^{\text{free}} = +0,341(46)\%$, $g_D = 2,0020(1)$. The authors deposited Ne/H₂ and Ne/D₂ mixtures on a cold substrate at 4–9 K. During matrix deposition a continuous microwave discharge at 10–90 W power levels was maintained in a 9 mm o.d. fused silica tube. Close analysis of the experimental technique and obtained results prove that either all the atomic-component fraction or the major part of it is produced in the solid Ne layer in situ. This is due to electron bombardment from the discharge and photolysis of the trapped H₂ molecules. Indeed, using the same set-up, the authors observed two trapping sites for hydrogen atoms in Ar and Kr, one of which was attributed to the substitutional site and the other — to the octahedral interstitial site. Until now, however, no studies are known which yielded interstitial hydrogen atoms in deposition experiments. The interstitial sites were reached only by atoms produced by some kind of irradiation of matrices containing trapped hydrogen molecules. In that case, the H or D atoms released during dissociation have enough energy to occupy an interstitial position. A direct evidence of this fact was provided by Miyazaki and co-authors [6] by observing EPR spectra of H atoms obtained in photolysis of Ar–H₂ mixtures (0.05 mol %) at 4 K. The number of interstitial atoms was found to increase significantly with increasing photon energy. The authors came to the conclusion that activation energy is required for trapping a hydrogen atom into an interstitial site. It was shown in experiments by Vaskonen *et al.* [7] that the relative numbers of the substitutional and interstitial atoms obtained by in situ photolysis depend also on the sample quality: deposition at very low temperatures or rapid freeze of liquid samples result in increased number of substitutional atoms in photolysis experiments. The discharge tube in the experiments by Knight *et al.* [5] may be considered as an effective VUV lamp due to its large diameter, high discharge power supplied. Also the authors stressed that “...the visible part of the discharge extended approximately 10 cm from the microwave cavity to very near the end of the silica tube which was located 5 cm from the copper flat matrix deposition target”. The Ne discharge provides several intensive VUV radiation lines [8].

Molecular hydrogen can be dissociated in five distinct ways [9] by photons with energies from 14.7 to 31 eV. In the experiments by Knight *et al.* [5], trapped atoms could be produced not only by light irradiation but also by electron bombardment from the discharge region extended towards the substrate. Sheludiakov and co-authors [10] showed that trapped H and D atoms could be effectively produced in situ in solid molecular hydrogen by radio-frequency discharge run in helium vapor near the sample surface. They performed experiments at sample temperatures below 1 K and used weak pulsed discharge with duration of 0.01–0.3 ms and 20–30 Hz repetition rate in

order not to overheat the solid hydrogen film. They were able [11,12] to obtain samples with maximum H densities in H₂ films up to $2 \cdot 10^{19}$ cm⁻³, close to record values ever recorded.

H and D in solid Ne is a system interesting not only for theoretical reasons suggesting a new trap loading mechanism but also as an atomic source for trapping neutral atoms under special experimental conditions [13,14]. The proposed trap loading mechanism consists of magnetically capturing the low-energy fraction of paramagnetic atoms being released from the matrix, while the host Ne atoms stick to the walls. The method was tested by loading Cr [13], and Li atoms [15,16], as well as ⁷Li₂ dimers [17], and described in detail in a later publication [18]. The method's potential was verified theoretically by Bovino *et al.* [19]. The authors of the above loading technique hope [13,14] on reaching high H atom concentration in Ne of the order of 10⁻³, referring to a study by Fajardo *et al.* [20]. However, an estimate of impurity atom concentration, $10^{-6} < M < 10^{-3}$, reported by Fajardo and co-authors deals with Li atoms in heavy noble gases, Ar, Kr, Xe. One may see, from the short overview above, that it is a challenging issue to obtain H and D in solid Ne in large densities. Another feature substantially affecting the velocity distribution of hydrogen atoms after pulse matrix evaporation is the origin of the atom trapping sites in Ne and the lattice tension of the nearest matrix surroundings. This issue was discussed for Li in Ne [15,16]. Thus, obtaining large concentration of the substitutional H/D atoms with relaxed solid Ne surroundings is a crucial aim in developing the new technique of hydrogen atom loading into a magnetic trap.

Hyperfine coupling matrix shifts for H and D atoms in solid gases

The only experiments yielding H and D atoms, matrix isolated in Ne by the deposition technique, were reported by a scientific group of Ioffe Institute [21–23]. A very recent successful EPR study of H in Ne with the use of β -irradiation [24] will be discussed below in close connection with the deposition experiments. Being compared to each other, these two studies make clear the origin of the H(D) atom trapping sites in Ne. The experiments of the Ioffe Institute group are also the only ones presenting high-resolution EPR spectra of H and D in solid neon. Two gaseous flows were delivered to a fused silica substrate at liquid helium temperatures: a Ne/H₂ mixture was passed through radio-frequency (14 MHz) discharge and pure gaseous Ne avoiding the discharge. Both flows were cooled with liquid nitrogen.

Figure 1 shows the EPR spectrum of H atoms stabilized in solid Ne from the gas phase [21]. The spectrum consists of two doublets: a pair of narrow lines marked by *I*, and a pair of much broader lines with smaller hf splitting marked

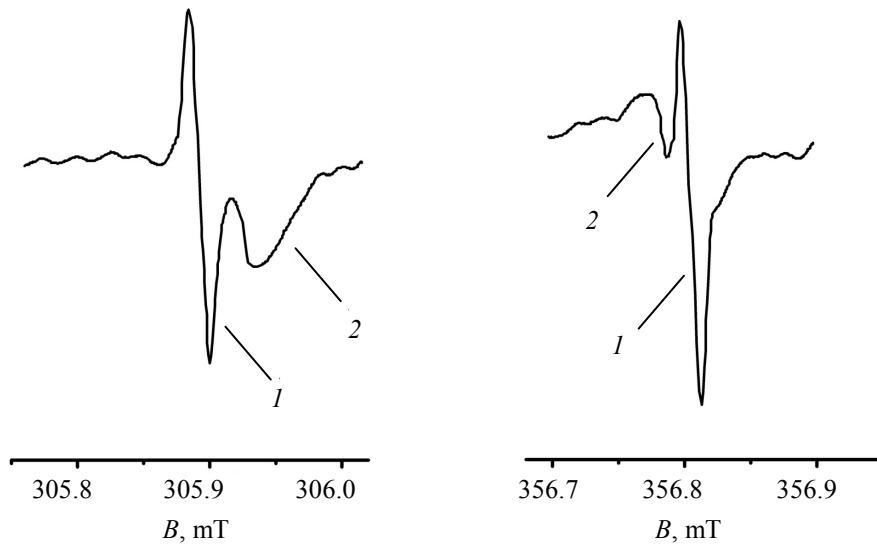


Fig. 1. Low-field and high-field lines of the EPR spectrum of H atoms trapped in solid Ne matrix deposited from the gas phase. The deposition was carried out on the substrate at $T_{\text{dep}} = 4.2$ K. The sample temperature during spectrum acquisition was $T_{\text{rec}} = 4.2$ K. The fraction of the molecular hydrogen impurity in the solid Ne matrix was estimated to $[\text{H}_2]:[\text{Ne}] \approx 2 \cdot 10^{-3}$.

by 2. The peak-to-peak linewidth of the hf components of the first doublet is 0.0090 mT, while the isotropic hf constant, g-factor, and relative matrix shift are $A = 1418.99(15)$ MHz, $g = 2.00210(8)$, and $\Delta A/A_{\text{free}} = -0.10(1)\%$. The matrix shift fits very well that of the substitutional H-atoms in Ne, $(\Delta A/A_{\text{free}})_{\text{theor}} = -0.09\%$ reported by Foner *et al.* [1] using a calculation method presented earlier by Adrian [25]. One expects narrow EPR lines of H in Ne because 99.7% of the natural neon consists of two even isotopes with nuclear spin magnetic moment equal to zero.

The parameters of the broad-line spectrum are, $A = 1417.4(2)$ MHz, $g = 2.00213(8)$, and $\Delta A/A_{\text{free}} = -0.21(2)\%$, while the linewidth is about 0.05 mT. A control experiment of similarly treated pure H_2 matrix was carried out in order to investigate if the molecular hydrogen impurities had something to do with the appearance of the broad-line

spectrum. It was found, that the H atoms were trapped in the solid H_2 matrix by condensation from the gas discharge. The obtained EPR parameters, $A = 1416.9(2)$ MHz, $g = 2.00221(8)$, $\Delta A/A_{\text{free}} = -0.24(2)\%$, were close to those of spectrum 2 in Fig. 1. The conclusion was thus drawn that spectrum 2 was due to hydrogen atoms trapped in the H_2 microcrystals formed under the quench condensation of the gaseous Ne- H_2 mixture [21]. Later on, however, further investigations were conducted on the structure of the binary hydrogen-neon solid mixture. The reader is referred to the next section of the present article for the analysis of the effect of the H_2/D_2 impurity concentration on the hydrogen atom trapping sites.

An unexpected result was obtained [22] in the trapping experiment of D atoms in Ne matrix seen in Fig. 2. A triplet of narrow lines numbered 1 has EPR parameters of:

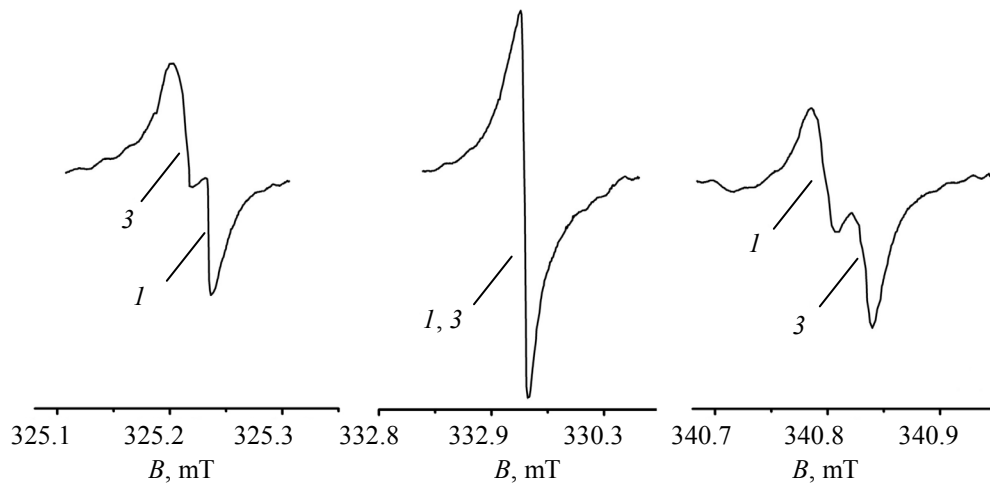


Fig. 2. EPR spectrum of D atoms trapped in solid Ne matrix from the gas phase. The deposition was carried out on the substrate at temperature $T_{\text{dep}} = 1.2$ K. Sample temperature during spectrum recording, $T_{\text{rec}} = 1.3$ K. The concentration of the molecular deuterium impurity in the solid Ne matrix is estimated to $[\text{D}_2]:[\text{Ne}] \approx 2 \cdot 10^{-3}$.

$A = 218.11(6)$ MHz, $g = 2.00208(8)$, $\Delta A/A_{\text{free}} = -0.07(3)\%$, and evidently may be linked to the spectrum *1* of hydrogen atoms of Fig. 1. However, the second multiplet, which is marked by number 3, also shows narrow lines. Moreover, the hf splitting is larger compared to spectrum *1*. The measured EPR parameters are as follows: $A = 218.98(6)$ MHz, $g = 2.00202(8)$, $\Delta A/A_{\text{free}} = +0.33(3)\%$. The gaseous deuterium used in the Ne–D₂ experiment contained 2% admixture of molecular hydrogen. The EPR spectrum of the hydrogen atoms was also observed during the same experiment consisting of only a narrow, 0.01 mT, doublet with parameters matching those of spectrum *1* in Fig. 1.

After the observation of the narrow triplet with positive shift of the hf-coupling constant, an experimental search was attempted for this type of H-atom centers. The spectrum was eventually recorded [23] in experiments with very small concentration of molecular hydrogen in gaseous Ne: with H₂/Ne ratios from 10⁻⁵ to 10⁻⁴, Fig. 3. The figure shows two narrow doublets numbered as *1* and 3. The matrix shift of the hf coupling constant of spectrum *1* is $-0.10(1)\%$, being thus identical to the spectrum *1* in Fig. 1. The measured shift of spectrum *3* is positive, $(\Delta A/A_{\text{free}})_{\text{theor}} = 0.40(1)\%$, and matches that of Foner *et al.* [1], obtained for H trapped in Ne in a photolytic experiment. The positively shifted HFC for H and D centers in Ne observed later by Knight *et al.* [5] coincided almost exactly with the above parameters.

Since the two H atoms trapping sites in Fig. 3 were obtained for very small concentration of H₂ in gaseous Ne, it was suggested that these two trapping sites would be observed also for D and H in one run if one performed experiments with extremely small concentration of D₂ in Ne. The suggestion was verified as the two trapping sites were found for D atoms as well as for H atoms in experiments with ex-

tremely dilute matrices obtained under [D₂]/[Ne] molar ratio of about 10⁻⁵ and very low deposition temperature.

Narrow line *1* and 3 spectra suggest that the particular H/D atom centers are trapped in surroundings of high regularity, e.g., substitutional or interstitial positions of the impurity atoms in the Ne crystal lattice.

Let us address to theoretical estimates of the HFC matrix shifts for hydrogen atoms in noble-gas solids. The first treatment was presented by Adrian [25] in 1960. It was assumed that the perturbing effect of the matrix consists of the van der Waals interaction which leads to a reduction in the HFC splitting and the Pauli exclusion forces leading to an increase in the splitting. These two opposite effects are treated separately and the results were summed up in order to obtain the net result. The model gives a satisfactory qualitative description of the shifts. Because the splitting is the difference between two competing effects that can only be roughly estimated, the quantitative estimates are rather sensitive to the approximations used. The ab initio calculation carried out by Kiljunen *et al.* [26] is an interesting and solid study. However, in certain cases, it provides theoretical hf constants which are not in sufficiently good agreement with the experimental findings. Indeed, the experimental matrix shift of the hf constant of the substitutional H-atom in solid Ar, -0.47% [23], turned out to be almost at midway between the Andrian's simple estimation [25] reported by Foner *et al.* [1], -0.72% , and the far more elaborated calculation by Kiljunen *et al.* [26], -0.26% . Both theoretical attempts differ from the measured value by about 50%. An even more discouraging theoretical result was found in [26] for the octahedral H in solid Xe: $+0.183\%$ compared to the experimental -1.09% [1], -1.02% [27], for "hot" hydrogen atoms obtained in photo-

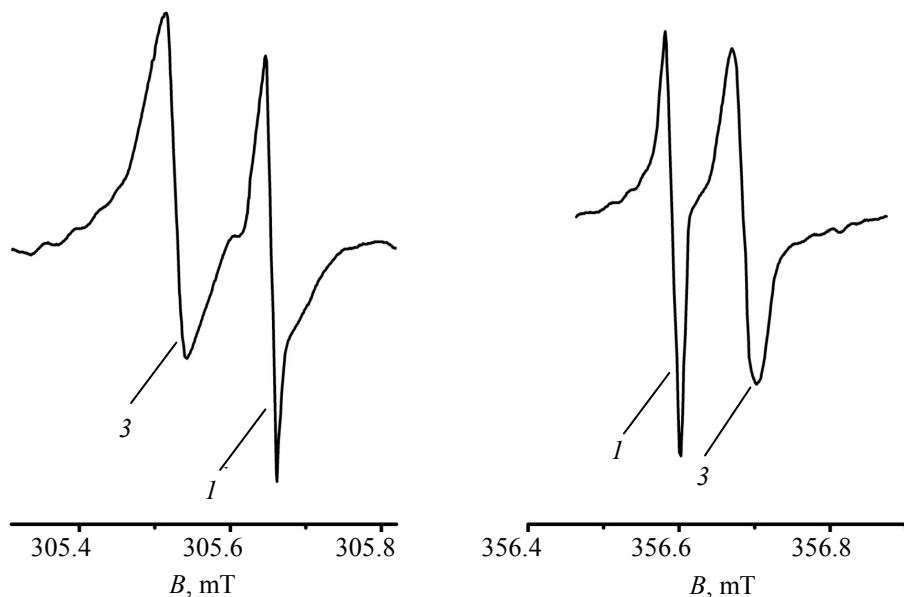


Fig. 3. The EPR spectrum of H atoms trapped in a solid Ne matrix from the gas phase. The deposition was carried out on the substrate at temperature $T_{\text{dep}} = 1.2$ K. The sample temperature during the spectrum recording was $T_{\text{rec}} = 4.2$ K. The fraction of the molecular hydrogen impurity in the solid Ne matrix was estimated by the ratio $[\text{H}_2]:[\text{Ne}] \approx 10^{-5}$.

lytic experiments, and -1.04% [1], -1.05% [28], in deposition experiments. For the substitutional H-atom, Kiljunen *et al.* [26] reported an estimate of $\sim -0.66\%$. Analysis of the experimental studies [1,28,29] made it clear, however, that deposited H-atoms are trapped in substitutional sites, while irradiated samples yield hydrogen atoms in the octahedral interstitial positions. By chance, the matrix shifts of the hf constants turned out to be identical in both the above cases. For the substitutional atoms, the theoretical estimate deviated from the experimental result by 37%. For H doped Xe lattice, the authors notified this obvious contradiction between experiment and theory. Here, we emphasize again the ab initio nature of the calculations by Kiljunen *et al.* which enables the experienced authors in obtaining theoretical predictions very close to the experimental data.

One small detail concerns the result for the interstitial H in Ar published by Foner *et al.* [1]. They reported $A = 1436.24(40)$ MHz, but 1.15% matrix shift instead of 1.115%. We notify that this misprint has been repeated by some other groups, e.g., by Kiljunen *et al.* [26].

Figure 4 gives hints about how well the theoretical results of the hf matrix shift for H atoms match the relevant experimental data in rare gas solids. With the exception of H/D in Xe, the theory allows discriminating substitutional H-atoms from interstitial ones, but the computed HFC matrix shifts for atoms in these sites is not that accurate. Amazingly, the theoretical estimates by Adrian [25] and Kiljunen [26] almost exactly reproduce the experimental data for the two possible sites of the H atom in solid Ne. To make a conclusion about the origin of these sites we undertook comparative analysis of the HFC matrix shifts for H in solid noble gases. Previously, we proposed [30] an empirical formula which links the isotropic hyperfine constants for methyl radical, CH_3 , in solid noble gases and para-hydrogen matrices to a particular linear combination of the van der Waals, E_V , and Pauli, E_P , energies. These energies involve the pair interaction between the impurity radical and the matrix particles. With large accuracy (the standard deviation was 0.02), the hyperfine constant was a linear function of $|E_V + 1.63 E_P|$. The correlation coefficient of the linear regression was measured to 0.99. It was shown later on [31,32] that the empirical formula works well (with correlation coefficient 0.98) for far vaster category of matrices including those of linear molecules: N_2 , CO , N_2O , CO_2 and also CD_4 , where additional attraction due to the anisotropic non-central interaction between the radical and the molecules should be taken into account. However, the relative weight parameter was found [32] to be larger, i.e., 2.73 instead of 1.63, due to corrected Lennard-Jones parameters (LJ) of the CH_4 - CH_4 interaction.

In the present study, we applied the same approach to the HFC matrix shift of H in solid noble gases. The attraction and repulsion energies were calculated on the basis of 6–12 Lennard-Jones potential [33,34].

$$V = \varepsilon \left[\left(\frac{R_{\min}}{R} \right)^{12} - 2 \left(\frac{R_{\min}}{R} \right)^6 \right].$$

Here, ε is the depth of the potential well, and R_{\min} is the equilibrium distance at the minimum of the typical 6–12 LJ potential. The negative (long-range) term gives attractive potential, $E_V = -2\varepsilon(R_{\min}/R)^6$, whereas the positive (short-range) one, the repulsive potential energy, $E_P = \varepsilon(R_{\min}/R)^{12}$.

Table 2 accumulates experimental data [44] on depth ε and equilibrium distances R_{\min} of the 6–12 LJ potential for the pair interaction between H atoms and matrix particles. Also given in the table are nearest neighbor distances, R_M , for atoms in the substitutional (“subst.”) and octahedral interstitial (“int.”) positions in pure crystal lattices of noble gases and H_2 (D_2) matrix [30,45] and calculation results for E_V and E_P . The columns 2, 3, 5, 6, 7 of Table 2 are reserved for H atoms. Column 3 accumulates results for pure solid noble gases and solid H_2 and D_2 matrices. The same distances are taken to be relevant for H atom impurities assuming no relaxation of the crystal lattice.

Several charts (not shown) such as the ones in Figs. 5(a) and 5(b) were plotted for the relative HFC matrix shifts of H and D in solid gases against $-(E_V + \beta E_P)$, where β is a parameter accounting for the weight of the Pauli repulsion. For each chart the standard deviation (SD) from the linear fit was measured and plotted in these figures as insets. On the basis of these plots, the values $\beta_{\min} = 1.79$ and 1.89, for H and D, respectively, were obtained when SD reached its

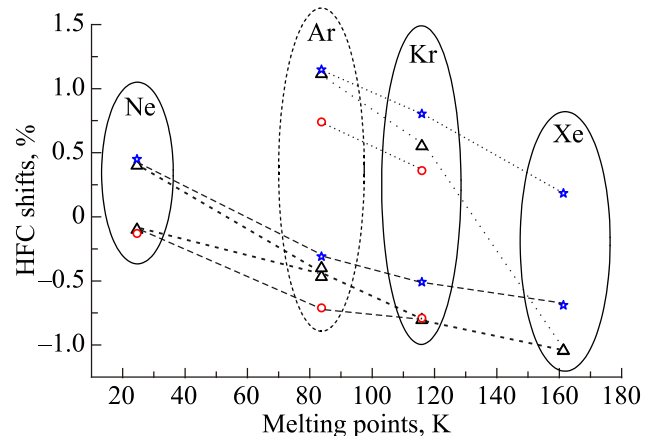


Fig. 4. HFC matrix shifts of H atoms in solid noble gases plotted against the melting points of the solids. Here, the triangles stand for the experimental results while the circles and the stars stand for the computations by Adrian [25] and Kiljunen *et al.* [26], respectively. Dashed and short dashed lines indicate results for the substitutional centers. The interstitial center results are tracked by dotted and short dotted lines. For the experimental results shown in this Figure see Table 1. Substitutional H/Ne and H/Ar data are taken from Ref. 23, interstitial H/Ar from Ref. 1, substitutional and interstitial H/Kr from Ref. 35 and Ref. 36, respectively, while substitutional and interstitial H/Xe are taken from Ref. 28 and Ref. 1, respectively.

Table 1. Isotropic hf splittings (MHz) and matrix shifts (%) of H and D data in solid gas matrices

	H		D		Refs.	Comment
	hf coupling	matrix shift, %	hf coupling	matrix shift, %		
Gas phase	1420.40573(5)		218.256201(20)		[1]	
Neon	1426.0(2)	0.394(14)	219.0(1)	0.341(46)	[5]	Hot*
	1426.11(15)	0.40(1)	218.98(6)	0.33(3)	[23]	Cold*
	1426.56(20)	0.433(20)			[1]	Hot
	1418.99 (15)	-0.10(1)	218.11(6)	-0.07(3)	[23]	Cold
	1419.0(3)	-0.10(2)			[24]	Hot
	1426.2(5)	0.40(3)			[24]	Hot
Argon	1435.7(3)	1.077(21)	-	-	[5]	Hot
	1436.24(40)	1.115(28)	-	-	[1]	Hot
	1416.31(80)	-0.288(56)	-	-	[1]	Hot
	1413.82(40)	-0.464(28)			[1]	Hot/Cold
	1413.0(2)	-0.521(14)	217.0(1)	-0.576(46)	[5]	Hot
	1413.74(11)	-0.469(8)	217.108(28)	-0.526(13)	[23]	Cold
	1414.7(2)	-0.40(2)	-	-	[23]	Cold
Krypton	1428(1)	0.535(70)	219.8(5)	0.707(229)	[5]	Hot
	1428.23(5)	0.551(3)	219.60(5)	0.616(23)	[36]	Hot
	1427.06(280)	0.468(20)	-	-	[1]	Hot
	1408,97(21)	-0,805(15)	-	-	[35]	
	1410.0(4)	-0.733(28)	216.2(3)	-0.942(137)	[5]	Hot
	1411.79(30)	-0.607(21)	-	-	[1]	Hot/Cold
Xenon	1404(2)	-1.155(141)	215.6(4)	-1.217(183)	[5]	Hot
	1405.70(5)	-1.035(3)	216.15(5)	-0.965(23)	[36]	Hot
	1405.55(38)	-1.046(27)	215.88(22)	-1.089(101)	[28]	Cold
	1404.99(28)	-1.085(20)	-	-	[1]	Cold
	1405.57(34)	-1.044(24)	-	-	[1]	Hot
Molecular deuterium	1416.7(2)	-0.26(2)	217.56(7)	-0.32(3)	[37]	Cold
	-	-	217.71(18)	-0.25(8)	[38]	Cold
	-	-	217.621(38)	-0.291(17)	[39]	Cold
	-	-	218.86(15)	0.277(69)	[40]	Hot
	1418.6(4)	-0.127(28)	218.08(15)	-0.081(69)	[40]	Hot
Molecular hydrogen	1417.11(20)	-0.23(14)	-	-	[38]	Cold
	1416.9(2)	-0.24(2)			[21]	Cold
Molecular tritium	1417.40(2)	-0,2116(14)	-	-	[41]	Hot
	1417.18(2)	-0.2271(14)	1512.60(2)	-0.2704(13)	[41]	Hot**
Molecular nitrogen	1415.24(26)	-0.364(19)	217.299(53)	-0.439(25)	[42]	Cold
	1434.063	0.962	-	-	[43]	Hot
	1415.520	-0.344	-	-	[43]	Hot

Notes: *The term “hot” here, stands for stabilized atoms obtained by any kind of the in situ irradiation of hydrogen containing species or bombardment from a discharge by non-thermalized H and D atoms. “Cold” stands for low-energy H and D atoms deposited from thermalized discharge plasma being in good thermal contact with cooled discharge tube walls.

**For tritium T atoms in T₂ matrix; $A_{\text{free}} = 1516.701471$ MHz, for the free T atom [41].

minimum. The results are presented in Figs. 5(a) and 5(b) and evidence fittings of excellent quality — the correlation coefficients were measured to 0.997 and 0.995, for H and D, respectively.

Graphs in Fig. 5 were plotted using -0.01% HFC matrix shift for H in Ne yielded by spectrum 1 presented in Figs. 1–3.

Figures 5(a) and 5(b), thus, evidence that the ground-state potential-energy curves and the distance dependent

Table 2. Literature data of intermediate parameters and computed values of attractive and repulsive potentials between an H atom and a matrix particle in various matrices^a

Matrix	$\varepsilon, 10^{-4} \varepsilon_0$	R_{\min}, a_0	R_M, a_0	$-E_V, 10^{-4} \varepsilon_0$	$E_P, 10^{-4} \varepsilon_0$	Trapping site
Ne	0.6983	5.858	5.95	1.272	0.5793	subst.
Ar	1.544	6.803	7.09	2.409	0.9401	subst.
Ar	1.544	6.803	5.013	5.229	4.428	int.
Kr	2.168	6.803	7.59	2.249	0.5829	subst.
Kr	2.168	6.803	5.367	5.889	3.998	int.
Xe	2.609	7.181	8.196	2.361	0.5339	subst.
Xe	2.609	7.181	5.795	18.89	34.17	int.
H ₂	0.7718	6.482	7.14	0.8639	0.2418	subst.
D ₂	0.7718	6.482	6.8	1.158	0.434	subst. ^b

Notes: ^aNearest neighbor distances, R_M , depth of the potential wells, ε , and equilibrium distance at the minimum of the typical 6–12 LJ potential, R_{\min} , versus the computed quantities of energies, E_V and E_P , for the pair interaction between trapped H atom and a matrix particle. Hartree atomic units are utilized for relevant quantities: $\varepsilon_0 = 27.212$ eV unit of energy, $a_0 = 0.52918$ Å unit of length. Parameters of the pair interaction potentials between D atoms and matrix particles were set equal to those of H atoms.

^bResults are presented for D atom in D₂ matrix.

shifts of the isotropic HFC in matrices are rather similar in shape. This was also suggested by Kiljunen *et al.* [26]. By a slight modification of the H/D-matrix particle pair potential function an excellent fit of the HFC matrix shifts was obtained, Figs. 5(a) and 5(b). Because of the excellent fitting of the experimental points, one may suggest that the function $E_V + \beta E_P$ describes reasonably well the distance to the nearest neighbors dependence of the HFC matrix shifts. In Figs. 6–10, this empiric dependence is correlated to the results by Adrian [25] and Kiljunen *et al.* [26].

For the Ne matrix, Fig. 6, the empirical curve is amazingly close to the Adrian’s result, while in the other matrices it correlates better with the ab initio computation by Kiljunen *et al.* The HFC matrix shift of the Ne⁽³⁾ H/D atom centers does not fit to the linear dependence in Figs. 5(a) and 5(b). This is evident from Figs. 11(a) and 11(b) where the experimental results for H/D in solid N₂ are also shown, Table 1, testifying that the empirical linear dependence fits well results in a vast category of gas solids. The

van der Waals interaction energy, E_V , between H and N₂ was estimated as $E_V \approx -\frac{C_6}{R^6}$, where $C_6 = 21\varepsilon_0$ [44]. By

considering the balance of E_V and E_P terms of the Lennard-Jones potential, the unknown repulsive potential energy was estimated by the relation $E_P = \left(\frac{E_V}{2}\right)^2 \cdot \frac{1}{\varepsilon}$. In ad-

dition, the well-known empirical mixing rule [46] may give the depth of the potential well, ε_{AB} , for two different interacting particles, A and B , in the form of the geometric mean of the depths of the involved pure substances, $\varepsilon_{AB} \approx \sqrt{\varepsilon_A \times \varepsilon_B}$, where ε_A and ε_B are the depths for $A-A$ and $B-B$ potentials. Therefore, ε can be expressed as $\varepsilon \approx \sqrt{\varepsilon_H \times \varepsilon_M}$, where ε_M is the depth of the potential energy well between the matrix, M , particles. For ε_H we used $5.27 \cdot 10^{-5} \varepsilon_0$ estimated from H–Ar, 4.2 meV, and Ar–Ar, 12.3 meV, interaction potentials [44]. Here, we address to the fact

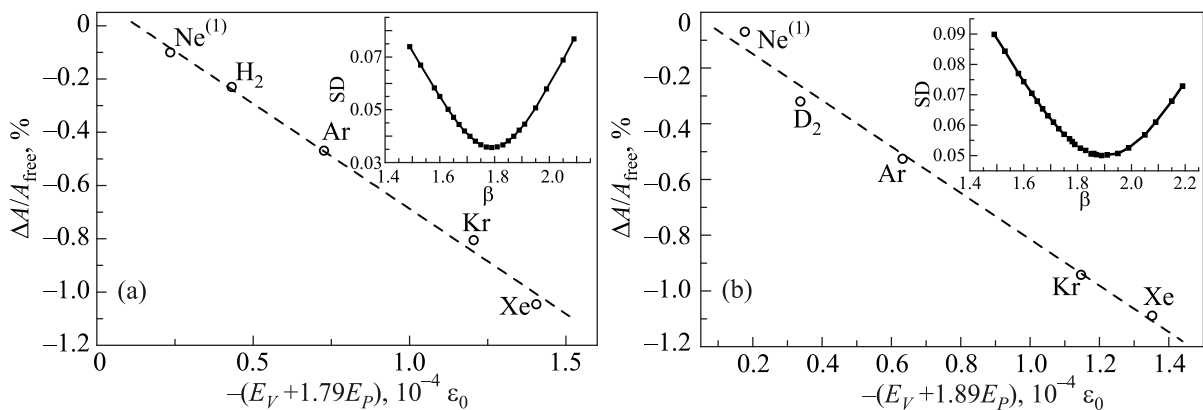


Fig. 5. Plot of the HFC matrix shift of substitutional H atoms against the usual solid gas hosts showing the effect of the van der Waals attraction and the Pauli repulsion (a). Plot of the HFC matrix shift of substitutional D atoms against the usual solid gas hosts showing the effect of the van der Waals attraction and the Pauli repulsion (b).

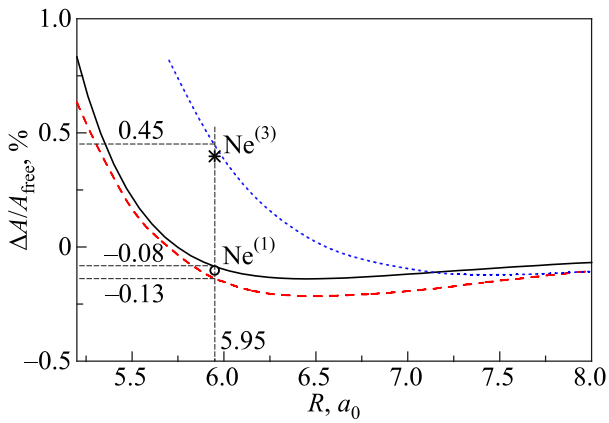


Fig. 6. (Color online) The HFC matrix shift vs. the distance to the nearest neighbors of the H atoms in solid Ne. Here, the empirical result of the present study is represented by the black solid line, the red dashed and the blue dotted curves come from the computations by Adrian [25] and Kiljunen *et al.* [26], respectively. The experimental results, Fig. 3, are indicated by the open circle and the star and are attributed to the substitutional H atoms.

that solid Ar is very close in physical parameters to solid N₂. Given this estimation and the N₂–N₂ potential [45], 8.2 meV, the H–N₂ potential well was obtained: $1.26 \cdot 10^{-4} \epsilon_0$.

Figures 11(a) and 11(b), thus, suggest that the H/D center in Ne with positive shift, commonly in the literature assumed as substitutional impurity in regular Ne lattice, is, actually, a substitutional center in some relaxed Ne surroundings. We address to its origin in the next section. It is also seen from Figs. 11(a) and 11(b) that the negatively shifted EPR spectrum *I* in Figs. 1–3 is related to the H/D atoms trapped substitutionally in the regular Ne lattice.

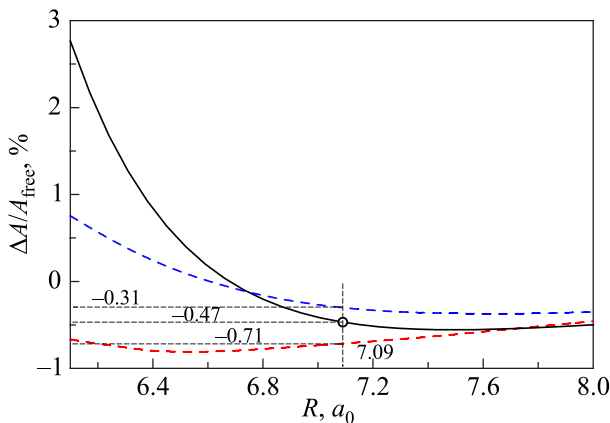


Fig. 7. (Color online) HFC matrix shift vs. the distance R to the nearest neighbors for H in solid Ar. Here, the empirical result of the present study is the black solid line, the red dashed and blue dotted curves are representing the computations by Adrian [25] and Kiljunen *et al.* [26], respectively. The measured HFC matrix shift [23] is indicated by the open circle (○) and is attributed to the substitutional H atoms.

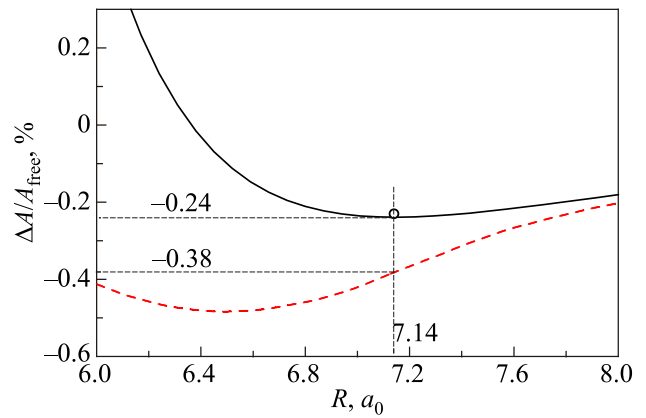


Fig. 8. (Color online) HFC matrix shift vs. the distance to the nearest neighbors for H in solid H₂. Here, the empirical result of the present study is represented by the black solid line, while the red dashed curve is the result of the computations according Adrian [25]. The measured HFC matrix shift [38] is indicated by the open circle (○) and is attributed to the substitutional H atoms.

Therefore, the present analysis testifies that the empirical linear dependence of the H and D relative HFC shifts on the particular linear combinations of E_V and E_P interaction energies works satisfactorily for the substitutional atoms, i.e., near the minima of these E_V and E_P combinations as functions of R , which is seen in Figs. 6–10. The EPR data for the interstitial hydrogens available from the literature may verify the applicability of this approach for short distances where the repulsion between the H/D atom and the matrix particles takes much over the attraction. In Fig. 12, the doubled experimental shifts [1,36] for the interstitial (octahedral) H atoms in noble gas solids are shown together

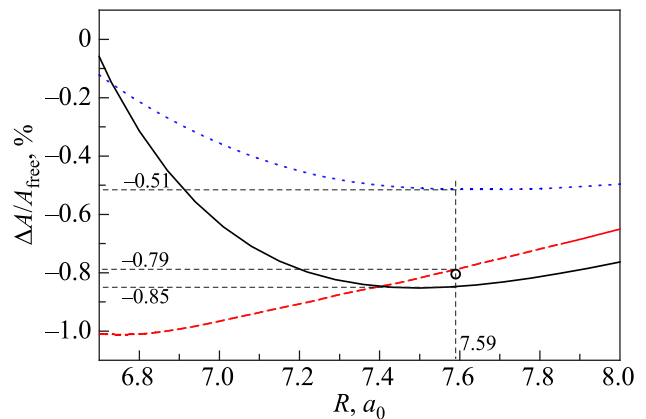


Fig. 9. (Color online) The HFC matrix shift vs. the distance to the nearest neighbors for H atoms isolated in solid Kr. Here, the empirical result of the present study is represented by the black solid line, red dashed and blue dotted curves are the computation results by Adrian [25] and Kiljunen *et al.* [26], respectively. The measured HFC matrix shift [35] is indicated by an open circle (○) and is attributed to the substitutional H atoms.

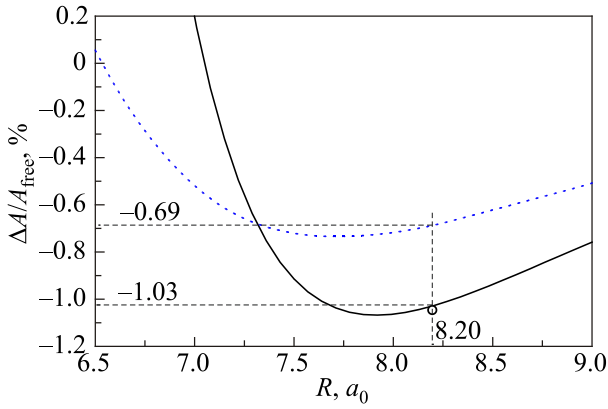


Fig. 10. (Color online) HFC matrix shift vs. the distance to the nearest neighbors for H in solid Xe. Here, empirical result of the present study is in black solid line, while a blue dotted curve is for the computation by Kiljunen *et al.* [26]. Measured HFC matrix shift [28] is indicated by an open circle and is attributed to the substitutional H atoms.

with the relative shifts for the substitutional atoms. The multiplication by two owns to the fact that a substitutional impurity in the FCC (face cubic centered) lattice has 12 nearest neighbors while an octahedral impurity has only half of them, i.e., 6 neighbors. In Fig. 12, the substitutional experimental results for the Ne regular lattice from Fig. 5(a) and Fig. 11(a) are shown to fit linearly (dashed line) the interaction energies E_V and E_P combined to $E_V + 1.79E_P$.

The open triangles correspond to the repulsion and the attraction felt by the octahedral interstitial H atoms in a regular crystal lattice in noble gases. The theoretical study by Kiljunen *et al.* demonstrated that the host matrix experiences relaxation because the matrix particles are pushed outward by the trapped octahedral H atom. The relaxation was estimated [26] to be in Ar 12%, in Kr 7%, and in Xe 3%. As a result, the corrected abscissas move the experimental HFC shifts much closer to the substitutional fitting line. Grünberg and Gabriel [47] used several accurately measured noble gas-hydrogen pair potentials to calculate the host lattice relaxation pattern produced by hydrogen atom impurities at substitutional and octahedral interstitial sites in rare gas crystals. The displacements range from 10% to 16% of the unrelaxed distances in H/Ar and from 6% to 10% in H/Xe. The partially filled triangles in Fig. 12 correspond to the maximum reductions according to Grünberg and Gabriel.

It seems from the above analysis, that the present empirical approach overestimates somewhat the positive HFC shift contribution from the repulsion at short distances between trapped atoms and matrix particles. Also, Figs. 6–10 suggest a faster HFC shift increase with decreasing matrix-impurity-species distance R predicted by the empirical approach compared with the Adrian’s and

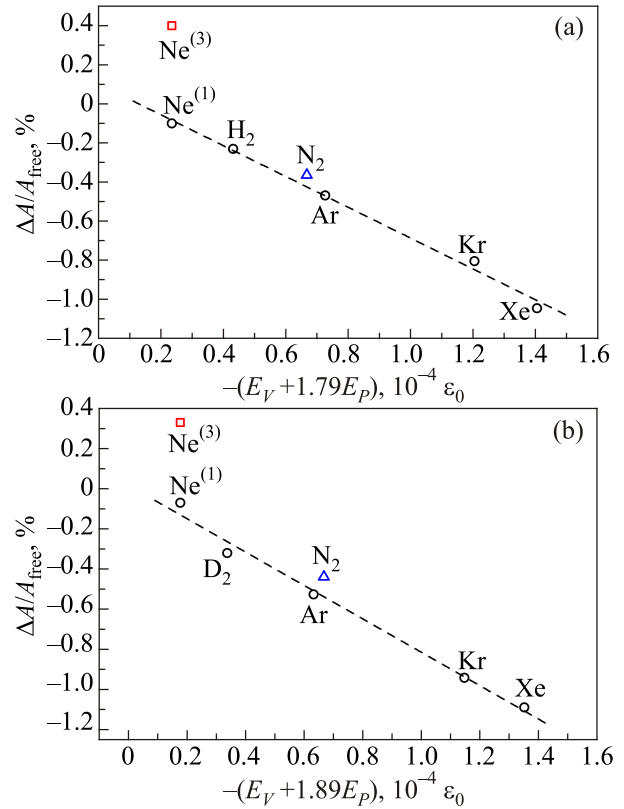


Fig. 11. (Color online) HFC matrix shifts of substitutional H atoms in solid gases affected by both van der Waals attraction and Pauli repulsion. The matrix shift obtained from doublet 3 for H in Ne, Fig. 3, is indicated by the red square. Shown by the blue triangle, is an experimental result for the substitutional H in N_2 , Table 1, to testify the applicability of the empirical fitting line in a vaster category of matrices (a). HFC matrix shifts of substitutional D atoms in solid gases affected by both van der Waals attraction and Pauli repulsion. The matrix shift obtained from doublet 3 for D in Ne, Fig. 2, is indicated by the red square. Shown by the blue triangle, is an experimental result for the substitutional D in N_2 , Table 1, to testify the applicability of the empirical fitting line in a vaster category of matrices (b).

Kiljunen *et al.* theories. The latter theory by Kiljunen *et al.* [26] predicts in addition an abrupt turn-over of the spin density and a Fermi contact term which indicates extensive shielding of the proton from the unpaired electron at very short distances. An indication of this turnover is also seen from Adrian’s computation [25] for H in Ar. Evidently, the present empirical approach does not account for this effect. On the other hand, it gives an excellent estimate for the substitutional H/Xe HFC shift. Notice however, that all the above three approaches fail to reproduce the octahedral H/Xe HFC shift in any satisfactory degree. We suppose that this effect deals with a rather considerable admixture of the ionic $Xe^+ \dots H$ -component into the covalent $Xe \dots H$ “molecule” [36].

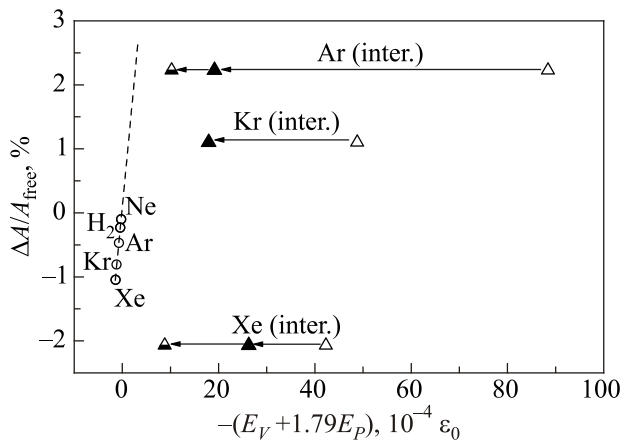


Fig. 12. Multiplied by two (doubled) experimental shifts for interstitial (octahedral) H atoms in noble gas solids [1,36], triangles, are shown together with the relative shifts for the substitutional atoms, open circles. The above multiplication by 2 owns to the fact that a substitutional impurity in the FCC (face cubic centered) lattice has 12 nearest neighbors while an octahedral impurity has 6 neighbors. The dashed line fits the substitutional experimental results in Fig. 5(a) and Fig. 11(a). The arrows pointing to the left show the reduction in the matrix atom -hydrogen interaction which follows lattice relaxation.

Concentration effects and trapping sites of H and D in solid Ne

Another issue showing the striking difference between the 1 and 3 EPR spectra of H/D in Ne is due to the isotope effect in the HFC relative matrix shifts which is evident from Table 1. A qualitative approach was suggested earlier [37,48] to explain the isotope effect. Setting $\delta A = (A/A_{\text{free}})^{\text{H}} - (A/A_{\text{free}})^{\text{D}}$ as a measure of it, it was found that δA has different sign for different centers: positive, for the substitutional H/D in Ar, D₂, T₂, Kr, N₂, and negative, for the substitutional H/D in Ne, spectrum 1, and octahedral

H/D in Kr. The qualitative explanation [37] of the sign change was in satisfactory agreement with the experimental results, based on the Adrian's curves for the HFC dependence on the matrix-impurity-species distance R . The δA sign should be related to the derivative of the above dependence of HFC on R , and, therefore, it should be negative for both the 1 and 3 H/D centers in Ne. In contrast to that assumption however, the spectra 3 yielded positive δA , Table 1.

The concentration of molecular hydrogen in solid Ne has significant effects on the trapping sites of H (D) atoms and, hence, also, on the ESR spectra, as seen from the experimental data collected in Table 3.

In the deposition experiments, H and D centers with positive hf constant shifts were obtained at the smallest possible experimental concentrations of molecular H₂ and D₂ in mixtures with Ne: $[H_2]/[Ne]$ from 10^{-5} to 10^{-4} , $[D_2]/[Ne] \approx 10^{-5}$. At fractions $[H_2]/[Ne]$ from 10^{-4} to 10^{-2} the centers with the positive shift disappear, while a spectrum attributed to H in H₂ microcrystals emerges. At fractions $[H_2]/[Ne] > 10^{-2}$ no H centers are observed with the exception of those trapped in solid H₂ regions. Note that in the D₂/H₂/Ne mixtures, H₂ constitutes 2% of the D₂ content.

The crystal structure of H₂/Ne films was studied by x-ray diffraction [49–51]. The samples were obtained by quench-condensation of the gaseous mixture on a 5 K substrate. The Ne–H₂ system is considered as nearly isotope mixture because of the close similarity of the Lennard-Jones parameters of the components: $\sigma = 2.788 \text{ \AA}$, $\epsilon = 36.7 \text{ K}$ for solid Ne, and $\sigma = 2.96 \text{ \AA}$, $\epsilon = 36.7 \text{ K}$ for solid H₂. The greatest discrepancy is in the mass and, hence, the degrees to which the components retain their quantum nature differ substantially. Consequently, the difference of the molar volumes of the crystals of the pure components is also large [51]. Because of this, the mutual solubility of the components is very limited: the maximum solubility of H₂ is only 0.5% when Ne–H₂ mixtures crystallize from the liquid phase [52]. However, at quench deposition, the re-

Table 3. The experimental temperature conditions and the molar ratios of hydrogen molecules to Ne matrix atoms in EPR active D₂/H₂/Ne mixtures

H ₂ /D ₂ concentration in Ne	Gaseous mixture delivered onto the substrate	Atoms under investigation	Spectra recorded at the substrate temperature during deposition, T_{dep} , K	
			4.2	1.2–1.6
$\geq 10^{-2}$	H ₂ /Ne	H	-	spectrum 2
10^{-2} – 10^{-4}	H ₂ /Ne	H	spectrum 1 spectrum 2	spectrum 1 spectrum 2
	D ₂ /H ₂ /Ne	H D	no no	spectrum 1 spectrum 1 spectrum 3
10^{-4} – 10^{-5}	H ₂ /Ne	H	no	spectrum 1 spectrum 3
	D ₂ /H ₂ /Ne	D	no	spectrum 1 spectrum 3

gions of single-phase solutions based on the initial components can be much wider than the nominal limits. Gal'tsov *et al.* [51] performed x-ray investigation of the solid solutions formed by condensation of mixtures of normal hydrogen and neon gases for concentrations ranging from 2 to 60 mol % $n\text{H}_2$ and temperatures ranging from 5 K to the melting temperature of the sample. The authors reported that for all mixtures up to 60 mol % $n\text{H}_2$ the reflections attributable to the hydrogen hcp phase (hcp_1) were not observed. They found that at large H_2 concentrations, except the *fcc* structure a new hcp_2 phase was formed with a lattice volume close but somewhat larger than the volume of pure Ne: 13.5, 13.4, 13.3 cm^3/mole , for *fcc*, hcp_2 , and pure neon, respectively. The boundary of single-phase solutions of hydrogen in neon was established to 2 mol %. The authors stressed that the hcp_2 phase is an excellent hydrogen accumulator and, as an upper limit, it can contain up to 83 mol % H_2 . For 1 mol% H_2 -Ne mixture, the x-ray investigation showed neither hcp_2 structure formation nor H_2 microcrystals [51]. Spectrum 2, Fig. 1, cannot be attributed to H in the hcp_2 phase which is rich in molecular hydrogen. Indeed, the closeness of the lattice volumes of the pure Ne and the hcp_2 molecular crystals suggests that the distance from the substitutional H atom to the nearest matrix particle should be nearly equal 3.1 Å, the nearest neighbor distance for pure Ne. At such a small distance, the contribution from the nearest H_2 molecule to the HFC matrix shift should be positive disagreeing with the experimental negative shift measured for the EPR spectrum 2. Hence, the small line width as well as the negative HFC shift suggest that spectrum 2 is attributable to H atoms trapped in the H_2 microcrystals.

Thus, the EPR investigation of quench-condensed mixture films shows formation of the pure H_2 solid phase in these films for very small gas phase fractional impurity concentration of H_2 to Ne down to 10^{-4} when deposition is performed on the substrate at 1.2 K. The EPR spectroscopy with the H-atom as a probe turned out to be a very sensitive technique to discriminate the H_2 single-state phase (regions of pure H_2) which is not observable by the x-ray technique, probably because of small size and/ or low concentration of molecular H_2 clusters.

A very recent EPR study by Sheludiakov *et al.* [24] provides solid evidence that the pure H_2 clusters are formed in solid Ne when gaseous Ne/ H_2 mixture with 10^{-4} concentration of molecular hydrogen is deposited onto a substrate at 0.8–1.3 K. This solid mixture subjected to β -irradiation yielded three EPR doublets of stabilized H atoms — two with negatively shifted HF constants and one with a positively shifted constant. The centers with $(\Delta A_H)/A_H^{\text{free}}$ equal to $-0.10(2)\%$ and $+0.40(3)\%$ hit exactly the HF splittings of the $\text{Ne}^{(1)}$ and $\text{Ne}^{(3)}$ doublets obtained in the deposition experiments, Table 1. The third doublet exhibits negative HFC matrix shift, $-0.19(3)\%$, and linewidth, 0.8 G, close to that of H in pure H_2 recorded with the same set up:

$-0.21(1)\%$ and 1.0 G, respectively. The relative intensity of this doublet increased with increasing admixture of H_2 in Ne. The low temperature of the substrate and low deposition rate of 0.1 monolayers/s [53] resulted in very high porosity of the sample with specific surface area, $\sigma = 145 \text{ m}^2 \cdot \text{g}^{-1}$. Thus, the H_2 clusters may be confined inside the pores following the restricted geometry conditions. The authors observed [24] abrupt recombination of H atoms in H_2 clusters upon the sample heating from 0.1 to 0.6 K. This effect occurs due to the solid-to-liquid transition of the clusters. The hydrogen molecule interaction with the Ne cage around a cluster reduces effectively the H_2 - H_2 attraction forces, lowering thus the temperature of the solid-to-liquid phase transition. Considering this effect, one may conclude that the efficient $E_V + 1.79E_P$ abscissa value in Fig. 5(a) becomes smaller for the H_2 clusters compared to the bulk H_2 , leading to H atom HFC value closer to the free atom. The measured mean HFC matrix shifts of -0.21% and -0.19% do not contradict this suggestion.

The rich in molecular deuterium Ne hcp_2 structure in Ne/ D_2 samples was observed by Belan *et al.* [54] in an x-ray investigation of binary Ne- $n\text{D}_2$ mixtures condensed on a substrate at 5 K. The authors found that, because of the smaller difference in the masses of the components for the Ne- D_2 mixture compared to Ne- H_2 , the region of the mutual solubility of the former mixture is almost two times wider than the latter. With increasing D_2 concentration in Ne, the hcp_2 phase starts to appear at mol fraction $x = 4.5\%$, which is the low concentration limit compared to the corresponding mol fraction $x = 2\%$ for the hcp_2 appearance in the Ne- H_2 mixture. This observation also suggests a greater solubility of the heavier hydrogen isotope, D_2 , in solid Ne. On the basis of the EPR line width, the spectrum 3 in Fig. 2 cannot be due to D atoms trapped in the Ne hcp_2 phase. The line width of D in solid D_2 obtained in deposition experiment is 0.13 mT [55] and is attributable to the superhyperfine broadening. Let us take into consideration that the EPR line width is proportional to the square root of the number of the nearest matrix molecules and inversely proportional to the third power of the nearest neighbor distance [56]. Adjusting the 0.13 mT width by the opposite operations it is estimated that even one nearest D_2 molecule would

broaden the line to $\frac{0.13}{\sqrt{12}} \cdot \left(\frac{3.6}{3.1}\right)^3 = 0.06 \text{ mT}$. Here, 3.6 Å is

the nearest neighbor distance for solid D_2 [45]. Thus, the expected line width for D stabilized in the Ne hcp_2 structure is far above the measured 0.018 mT [23].

In Ne/ D_2 experiments with 1% D_2 in gaseous Ne, no broad lines with negative HFC shift originating from D trapped in D_2 microcrystals were recorded. This finding is in line with the results by Belan *et al.* [54] on larger solubility of D_2 in Ne compared to H_2 . Note also the failure to obtain matrix isolated D in Ne at substrate temperature 4.2 K. Only low temperature substrate in the range 1.2–1.6 K was

efficient in trapping deuterium atoms, Table 3. This is an unexpected result because, normally, the heavier D atoms were believed to be trapped easier than the lighter H atoms.

The experimental results under discussion in the present study allow us to suggest a trapping H/D atoms mechanism in solid Ne from the gaseous phase. The collisions between the H atoms and the matrix particles (Ne or H₂) are governed by the energy and momentum conservation laws. The H-atom loses $8/9 = 0.89$ of its initial kinetic energy in case it impacts a H₂ molecule, while only $1 - (19/21)^2 = 0.18$ in the collision with a Ne atom. This follows from the kinematic ratio:

$$E = E_0[4 m_1 m_2 / (m_1 + m_2)^2] \quad (1)$$

with m_1 and m_2 the masses of H(D) atom and matrix particle, respectively; E_0 the hydrogen atom kinetic energy; E the energy of the particle on the surface after a collision with a H(D) atom. This simple model may be used for crude estimation of the energy transfer during the atom-surface collision [57]. It shows that the H atom is hard to accommodate on the Ne surface because of the small H–Ne interaction potential depth and the semiquantum nature of the solid Ne. It is reasonable that if there is a large mismatch between the mass of the incoming atom and the atom(s) of the surface, the transfer of energy is inefficient and the atom might bounce a few times on the surface before it becomes trapped [58] or repelled. Bouncing along the Ne surface, H/D atom encounters H₂-reach regions to loose efficiently its excess kinetic energy and become trapped in the H₂ microcrystal or in the nearest pure Ne regions. Thus, because of the incomplete solubility of H₂ in Ne and the complete solubility of D₂ at concentrations below 1%, the spectrum 2 of H/ H₂ is observable in the experiment while that of D/ D₂ is not. This is also the reason of the fact that the spectrum 1 of H in Ne shows up in deposition on the 4.2 K substrate while the spectrum 1 of D in Ne does not. Bernard *et al.* [39] performed EPR experiments with an 1:4 Ne to D₂ mixture passed through a rf discharge diluted by excess gaseous He. This plasma jet was introduced into a volume of superfluid helium directly through its surface. The EPR recording yielded only the D/D₂ triplet and no D atom centers in solid Ne. The x-ray diffraction technique that the authors employed in this experiment showed, however, formation of both D₂ and Ne clusters. Correlating the EPR to the x-ray observations, we came to the conclusion that the D₂ clusters scavenge the entire D atom fraction while the Ne clusters — nothing.

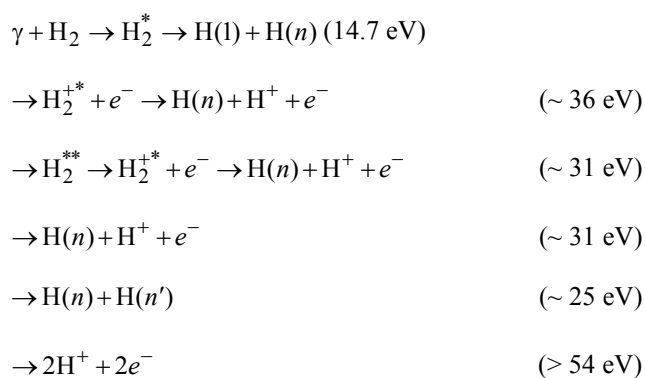
The experiment by Sheludiakov and colleagues [24] is the first irradiation H–Ne EPR study where the HFC negatively shifted Ne⁽¹⁾ H atom doublet is found. Simultaneously they obtained that the HFC positively shifted Ne⁽³⁾ H atom doublet is much more intensive than the Ne⁽¹⁾ at all H₂/Ne concentrations tested in the study. Both H atom centers in Ne yielded much broader lines compared to the deposition experiments: 1.3 and 1.8 G for Ne⁽¹⁾ and Ne⁽³⁾ centers, respectively. Sheludiakov *et al.* carried out exper-

iments at the one order of magnitude higher magnetic field of 4.6 T, compared to the field used in the deposition experiments: 0.33 T. For the sake of comparison, we made a crude estimation of the line widths recorded in experiments by the Turku University group and the Ioffe Institute group. We concluded that most of the broadening came from the distribution of the g -factor parameters of the H atoms due to variable disorder of the local atomic Ne surroundings. It was namely found previously that the g strain and not the A strain is the main reason of the EPR broadening of CH₃ in Kr [59]. Accordingly, the widths of 1.3 and 1.8 G at 4.6 T were adjusted to the lower magnetic field as 0.093 and 0.129 G, respectively, in good agreement with the widths 0.09 and 0.15 G, reported by the Ioffe Institute group [23]. Both groups, thus, reported broader Ne⁽³⁾ central lines than the Ne⁽¹⁾ ones. This difference suggests that the Ne⁽¹⁾ centers relate to nearly undisturbed substitutional sites in the regular Ne lattice, while the Ne⁽³⁾ centers feel some not fully reproducible, randomly relaxed, surroundings. A tentative origin of the Ne⁽³⁾ centers was discussed earlier. Foner and co-authors suggested that the Ne⁽³⁾ doublet is yielded by the substitutional H atoms with the neon matrix atoms drawn toward the H atom. However, the lattice contraction of 8%, in that case, is too large and is not in accord with theoretical estimates. Indeed, a calculation by Smith [60] shows 1.03% contraction, while Kiljunen *et al.* [26] estimated no contraction at all. Dmitriev and co-authors [23] considered stabilization of the Ne⁽³⁾ center in the vicinity of some lattice defect, i.e., edge dislocation, with a lattice contraction. On the other hand, this model suggests a closest surrounding of lower symmetry which would result in spectrum anisotropy.

The clue experiment in understanding the origin of the Ne⁽³⁾ centers was reported by Sheludiakov *et al.* [24] with annealed samples. The annealing was performed at 7–10 K with partial sublimation of the Ne film by ~ 10–15%. The lattice quality of the sample was tested by letting a quantity of He to be absorbed by nominally “pure” Ne (about 10⁻⁴ H₂ admixture) measured utilizing the quartz microbalance (QM) frequency shift. The QM frequency shift was 1500 Hz for the as-deposited sample and only 5 Hz for the annealed. The annealing, thus, led to the very regular Ne sample structure with small number of defects, vacancies included. Only the Ne⁽³⁾ centers were observed after irradiation in the annealed samples and no Ne⁽¹⁾ centers. Previously Vaskonen and co-authors [7] stressed that the ratio of population of the interstitial sites to that of the substitutional sites depends on the matrix quality and increases with increasing order. The origin of the Ne⁽³⁾ centers was suggested by Sheludiakov *et al.* [24] as being initially H atoms stabilized in octahedral interstitial voids of the Ne lattice and then relaxed to a position that is somewhat intermediate between the substitutional and interstitial. The complete structural relaxation for H in H₂ was first proposed by Li and Voth [61]. By virtue of Monte Carlo simulations,

they found that the zero point vibrations make solid hydrogen so compressible that the matrix cannot sustain the local stress created by interstitial impurities. As a result, the local environment for an impurity at an interstitial site is the same as that for an impurity at a substitutional site. The same effect of the complete relaxation of the surroundings was calculated for H in Ne by Kiljunen *et al.* [26] despite the fact that solid Ne is a semi-quantum matrix compared to the H₂ quantum solid: the de Boer parameter is 0.274 for H₂, versus 0.0918 for Ne. The experimental EPR results, however, suggest incomplete relaxation which may be estimated from Fig. 11(a). In order to have the Ne⁽³⁾ result on the fitting line in this figure, the nearest Ne atoms should be shifted outward a distance of *ca* 27.8% compared to 45.5%, in the case of complete relaxation. The number of matrix particles nearest to the trapped H atom is 12 in both models.

The origin of the Ne⁽³⁾ centers suggests that, in deposition experiments, these H atoms were obtained due to photolysis by the open discharge VUV light of H₂ and D₂ impurities in solid Ne which is the only matrix (aside solid He) where this process may be performed because of the high energy of the photons involved. This is evident from the reaction schemes [9,62] below.



Ne open discharge provides intensive VUV irradiation [8] at 16.8 eV (= 73.80 nm Ne_I component), 27 eV (= 45.92 nm Ne_{II} component), and several less intensive Ne_{II} components with energies up to 31 eV (= 39.99 nm).

Taking this model into account one may assume that the concentration effect on the Ne⁽³⁾ center appearance is due to suppression of the Ne_I and Ne_{II} irradiation by increased H₂ concentration in the H₂/Ne discharge.

Conclusions

The seemingly simple but still not fully understood H(D)/Ne system was considered in the present EPR-based study in some detail by comparing investigation results from deposition and irradiation experiments. An empirical approach was suggested which correlate the HFC matrix shifts of trapped H and D atoms to a certain combinations of the van der Waals and Pauli pair interactions between the impurity hydrogen atoms and the host matrix particles.

Impurity atoms, initially trapped in the octahedral interstitial sites, were relaxed to cramped substitutional positions, constituting the discovery of a new H(D) trapping mechanism supporting positive HFC matrix shifts.

It is worth pointing out that concentration effects in the hf-constant and g-factor of H atoms in H₂-Kr-He condensates were published previously by Boltnev and co-authors [63]. The EPR parameters varied nearly continuously with increased Kr content changing from those characteristic for H in pure H₂ to those characteristic of H in pure Kr. This effect was explained by the authors as thinning of the solid H₂ coating with trapped H atoms on the Kr nanocrystals. The concentration effect published here is of different origin. The present analysis of the concentration and temperature effects on the H/D trapping sites in Ne revealed a crucial role of the H₂ microcrystals impurity on the trapping efficiency. It was shown that the microcrystals are formed even at H₂ impurity concentration in the gaseous phase in the range 10⁻⁴-10⁻², where on the contrary, x-ray studies erroneously suggest complete solubility of the two components. However, D₂ microcrystals were not formed for concentrations up to 1% of D₂ in Ne, the largest D₂ impurity concentration in gaseous Ne utilized in the deposition experiments. The above HFC matrix shift analysis suggests that considerable lattice rearrangement is expected for H/D in Ne in general. The rearrangement may include lattice contraction accompanied by changing the lattice structure. A successful future theory applied to this system would involve the lattice relaxation and provide an explanation of the opposite HFC matrix shift isotope effect between the hydrogen (deuterium) in the observed, different 1 and 3 centers in solid Ne. Indeed, the isotope measure, $\delta A = (A/A_{\text{free}})^{\text{H}} - (A/A_{\text{free}})^{\text{D}}$ defined in the present work, is negative, $\delta A < 0$, for the Ne⁽¹⁾ H and D centers, while is positive, $\delta A > 0$, for the Ne⁽³⁾ H and D centers, indicating, respectively, smaller efficiency of the microcrystalline Ne⁽¹⁾ host on the HFC shift for the H atoms than for the D atoms and vice versa in Ne⁽³⁾.

1. S.N. Foner, E.L. Cochran, V.A. Bowers, and C.K. Jen, *J. Chem. Phys.* **32**, 963 (1960).
2. G. Baldini, *Phys. Rev.* **136**, A248 (1964).
3. V.E. Bondybey and G.C. Pimentel, *J. Chem. Phys.* **56**, 3832 (1972).
4. W. Böhmer, R. Haensel, N. Schwentner, and E. Boursey, *Chem. Phys.* **49**, 225 (1980).
5. L.B. Knight, Jr., W.E. Rice, L. Moore, E.R. Davidson, and R.S. Dailey, *J. Chem. Phys.* **109**, 1409 (1998).
6. T. Miyazaki, A. Wakahara, T. Usul, and K. Fueki, *J. Phys. Chem.* **86**, 3881 (1982).
7. K. Vaskonen, J. Eloranta, T. Kiljunen, and H. Kunttu, *J. Chem. Phys.* **110**, 2122 (1999).
8. J.E. Sansonetti and W.C. Martin, *J. Phys. Chem. Ref. Data* **34**, 1560 (2005).

9. R. Machacek, V.M. Andrianarijaona, J.E. Furst, A.L.D. Kilcoyne, A.L. Landers, E.T. Litaker, K.W. McLaughlin, and T.J. Gay, *J. Phys. B* **44**, 045201 (2011).
10. S. Sheludiakov, J. Ahokas, O. Vainio, J. Järvinen, D. Zvezdov, S. Vasiliev, V.V. Khmelenko, S. Mao, and D.M. Lee, *Rev. Sci. Instrum.* **85**, 053902 (2014).
11. J. Ahokas, O. Vainio, S. Novotny, J. Järvinen, V.V. Khmelenko, D.M. Lee, and S. Vasiliev, *Phys. Rev. B* **81**, 104516 (2010).
12. J. Ahokas, O. Vainio, J. Järvinen, V.V. Khmelenko, D.M. Lee, and S. Vasiliev, *Phys. Rev. B* **79**, 220505 (2009).
13. R. Lambo, C.C. Rodegheri, D.M. Silveira, and C.L. Cesar, *Phys. Rev. A* **76**, 061401 (2007).
14. P. Crivelli, C.L. Cesar, and R. Lambo, *Can. J. Phys.* **87**, 799 (2009).
15. R.L. Sacramento, L.A. Scudeller, R. Lambo, P. Crivelli, and C.L. Cesar, *J. Chem. Phys.* **135**, 134201 (2011).
16. R.L. Sacramento, B.X. Alves, D.T. Almeida, W. Wolff, M.S. Li, and C.L. Cesar, *J. Chem. Phys.* **136**, 154202 (2012).
17. A.N. Oliveira, R.L. Sacramento, B.X. Alves, B.A. Silva, W. Wolff, and C.L. Cesar, *J. Phys. B* **24**, 245302 (2014).
18. R.L. Sacramento, A.N. Oliveira, B.X. Alves, B.A. Silva, M.S. Li, W. Wolff, and C.L. Cesar, *Rev. Sci. Instrum.* **86**, 073109 (2015).
19. S. Bovino, P. Zhang, V. Kharchenko, and A. Dalgarno, *J. Chem. Phys.* **131**, 054302 (2009).
20. M.E. Fajardo, P.G. Carrick, and J.W. Kenney, *J. Chem. Phys.* **94**, 5812 (1991).
21. R.A. Zhitnikov and Yu.A. Dmitriev, *J. Exp. Theor. Phys.* **92**, 1913 (1987) [*JETP* **92**, 1075 (1987)].
22. Yu.A. Dmitriev and R.A. Zhitnikov, *Pis'ma v Zh. Tekhn. Fiz.* **14**, 661 (1988) [*Techn. Phys. Lett.* **14**, (1988)].
23. Yu.A. Dmitriev, R.A. Zhitnikov, and M.E. Kaimakov, *Fiz. Nizk. Temp.* **15**, 495 (1989) [*Sov. J. Low Temp. Phys.* **15**, 279 (1989)].
24. S. Sheludiakov, J. Ahokas, J. Järvinen, L. Lehtonen, S. Vasiliev, Yu.A. Dmitriev, D.M. Lee, and V.V. Khmelenko, *Phys. Rev. B* **97**, 104108 (2018).
25. F.J. Adrian, *J. Chem. Phys.* **32**, 972 (1960).
26. T. Kiljunen, J. Eloranta, and H. Kunttu, *J. Chem. Phys.* **110**, 11814 (1999).
27. G.S. Jeckel, W.H. Nelson, and W. Gordy, *Phys. Rev.* **176**, 453 (1968).
28. Yu.A. Dmitriev, *J. Phys. Condens. Matter* **5**, 5245 (1993).
29. V.I. Feldman, F.F. Sukhov, and A.Yu. Orlov, *J. Chem. Phys.* **128**, 214511 (2008).
30. Yu.A. Dmitriev and N.P. Benetis, *J. Phys. Chem. A* **114**, 10732 (2010).
31. Yu.A. Dmitriev, V.D. Melnikov, K.G. Styrov, and M.A. Tumanova, *Physica B* **440**, 104 (2014).
32. Yu.A. Dmitriev and N.P. Benetis, *J. Phys. Chem. A* **122**, 9483 (2018).
33. J.O. Hirschfelder, C.F. Curtiss, and R.B. Bird, *Molecular Theory of Gases and Liquids*, John Wiley & Sons (1966).
34. L. Zarkova, U. Hohm, and M.J. Damyanova, *Optoelectron. Adv. Mater.* **7**, 2385 (2005).
35. Yu.A. Dmitriev, *Fiz. Nizk. Temp.* **33**, 661 (2007) [*Low Temp. Phys.* **33**, 493 (2007)].
36. J.R. Morton, K.F. Preston, S.J. Strach, F.J. Adrian, and A.N. Jette, *J. Chem. Phys.* **70**, 2889 (1979).
37. R.A. Zhitnikov and Yu.A. Dmitriev, *Zh. Tekhn. Fiz.* **60**, 154 (1990).
38. C.K. Jen, S.N. Foner, E.L. Cochran, and V.A. Bowers, *Phys. Rev.* **112**, 1169 (1958).
39. E.P. Bernard, R.E. Boltnev, V.V. Khmelenko, V. Kiryukhin, S.I. Kiselev, and D.M. Lee, *Phys. Rev.* **69**, 104201 (2004).
40. M. Sharnoff and R.V. Pound, *Phys. Rev.* **132**, 1003 (1963).
41. S. Sheludiakov, *Magnetic Resonance Study of Atomic Hydrogen Stabilized in Matrices of Hydrogen Isotopes below 1 K*, PhD thesis, University of Turku, Turku (2017).
42. Yu.A. Dmitriev and R.A. Zhitnikov, *Fiz. Nizk. Temp.* **24**, 58 (1998) [*Low Temp. Phys.* **24**, 44 (1998)].
43. V. Shevtsov and N. Masaki, *Chem. Phys. Lett.* **244**, 188 (1995).
44. A.A. Radtsig and B.M. Smirnov, *Parameters of Atoms and Atomic Ions*, Energoatomizdat, Moscow (1986).
45. *Cryocrystals*, B.I. Verkin and A.F. Prikhotko (eds.), Naukova Dumka, Kiev (1983).
46. M. Layer, A. Netsch, M. Heitz, J. Meier, and S. Hunklinger, *Phys. Rev. B* **73**, 184116 (2006).
47. H.H. von Grünberg and H. Gabriel, *Chem. Phys. Lett.* **192**, 503 (1992).
48. Yu.A. Dmitriev and R.A. Zhitnikov, *Opt. Spectrosc.* **69**, 728 (1990).
49. A.S. Barylnik, A.I. Prokhvatilov, M.A. Strzhemechny, and G.N. Shcherbakov, *Fiz. Nizk. Temp.* **19**, 625 (1993) [*Low Temp. Phys.* **19**, 447 (1993)].
50. A.S. Barylnik, A.I. Prokhvatilov, and G.N. Shcherbakov, *Fiz. Nizk. Temp.* **21**, 787 (1995) [*Low Temp. Phys.* **21**, 607 (1995)].
51. N.N. Gal'tsov, A.I. Prokhvatilov, and M.A. Strzhemechny, *Fiz. Nizk. Temp.* **30**, 1307 (2004) [*Low Temp. Phys.* **30**, 984 (2004)].
52. C.S. Barrett, L. Meyer, and J. Wasserman, *J. Chem. Phys.* **45**, 834 (1966).
53. S. Sheludiakov, J. Ahokas, J. Järvinen, L. Lehtonen, S. Vasiliev, Yu.A. Dmitriev, D.M. Lee, and V.V. Khmelenko, *J. Low Temp. Phys.* (2018), online.
54. V.G. Belan, N.N. Gal'tsov, A.I. Prokhvatilov, and M.A. Strzhemechny, *Fiz. Nizk. Temp.* **31**, 1245 (2005) [*Low Temp. Phys.* **31**, 947 (2005)].
55. Yu.A. Dmitriev, *J. Low Temp. Phys.* **180**, 284 (2015).
56. Ch.P. Poole, Jr., *Electron Spin Resonance*, John Wiley & Sons, New York-London-Sydney (1967).
57. V. Voitsenya, D. Naidenkova, S. Masuzaki, Y. Kubota, A. Sagara, and K. Yamazaki, *J. Plasma Fusion Res. Ser.* **7**, 114 (2006).
58. G. Vidali, J. Roser, G. Manicó, V. Pirronello, H.B. Perets, and O. Biham, *J. Phys.: Conf. Ser.* **6**, 36 (2005).
59. Yu.A. Dmitriev, V.D. Melnikov, K.G. Styrov, and N.P. Benetis, *Physica B* **458**, 44 (2015).
60. D.Y. Smith, *Phys. Rev. A* **133**, A1087 (1964).
61. D. Li and G.A. Voth, *J. Chem. Phys.* **100**, 1785 (1994).

62. J.D. Bozek, J.E. Furst, T.J. Gay, H. Gould, A.L.D. Kilcoyne, J.R. Machacek, F. Martin, K.W. McLaughlin, and J.L. Sanz-Vicario, *J. Phys. B* **39**, 4871 (2006).
63. R.E. Boltnev, V.V. Khmelenko, and D.M. Lee, *Fiz. Nizk. Temp.* **36**, 484 (2010) [*Low Temp. Phys.* **36**, 382 (2010)].

Механізми і місця захоплення атомів H і D у твердому Ne

Yu.A. Dmitriev, N.P. Benetis

Зсуви для ізотропної контактної взаємодії Фермі (ІКВФ) для атомів водню і дейтерію, які ізольовані в кристалічних благородних газах при криогенних температурах, порівнюються з відповідними величинами для атомів H і D у газовій фазі. Нові експериментальні значення ІКВФ для H/D, захоплених у кристалічному Ne, порівнюються з експериментально отриманими і теоретично розрахованими значеннями. Можливі місця захоплення в спотвореній кристалічній структурі твердого Ne, які займають домішкові атоми водню, ідентифіковані за впливом на зсуви ІКВФ в спектрах ЕПР. Представлено обговорення залежності місць захоплення від процедури осадження матриці. ЕПР дослідження виявляють утворення мікрокристалітів H₂ в твердому Ne навіть при такому низькому, як 0,01% вмісті водню в осадженій H₂:Ne газовій суміші.

Ключові слова: ЕПР, водень, дейтерій, твердий Ne.

Механизмы и места захвата атомов H и D в твердом Ne

Yu.A. Dmitriev, N.P. Benetis

Сдвиги для изотропного контактного взаимодействия Ферми (ИКВФ) для атомов водорода и дейтерия, изолированных в кристаллических благородных газах при криогенных температурах, сравниваются с соответствующими величинами для атомов H и D в газовой фазе. Новые экспериментальные значения ИКВФ для H/D, захваченных в кристаллическом Ne, сравниваются с экспериментально полученными и теоретически рассчитанными значениями. Возможные места захвата в искаженной кристаллической структуре твердого Ne, занимаемые примесными атомами водорода, идентифицированы по влиянию на сдвиги ИКВФ в спектрах ЭПР. Представлено обсуждение зависимости мест захвата от процедуры осаждения матрицы. ЭПР исследование обнаруживает образование микрокристаллитов H₂ в твердом Ne даже при таком низком, как 0,01% содержании водорода в осаждаемой H₂:Ne газовой смеси.

Ключевые слова: ЭПР, водород, дейтерий, твердый Ne.